Extending the sensitivity of heavy sterile neutrino searches with solar neutrino experiments*

Yutao Zhu (朱宇涛)[1,2,3] Haoyang Fu (付昊阳)[1,2,3] Wentai Luo (骆文泰)[1,2,3] Shaomin Chen (陈少敏)[1,2,3]
Litao Yang (杨丽桃)[1,2,3] Zhicai Zhang (张志财)[1,2,3†]

[1]Department of Engineering Physics, Tsinghua University, Beijing 100084, China
[2]Center for High Energy Physics, Tsinghua University, Beijing 100084, China
[3]Key Laboratory of Particle & Radiation Imaging (Ministry of Education), Tsinghua University, Beijing 100084, China

Abstract: A sensitivity study of the search for heavy sterile neutrinos (ν_H) in the MeV mass range using solar neutrino experiments is presented. ν_H, with masses ranging from a few MeV up to approximately 15 MeV, can be produced in the Sun through ^{8}B decay and subsequently decays into $\nu_e e^+ e^-$. Its flux and lifetime strongly depend on the mixing parameter $|U_{eH}|^2$ and mass m_{ν_H}. The ν_H signal can be detected via its decay products, either the e^+e^- pair or ν_e, depending on whether ν_H decays inside or outside the detector. Expected signal yields for both detection methods (detecting e^+e^- or ν_e signal) are presented across the full $|U_{eH}|^2$ and m_{ν_H} parameter spaces. These two methods are found to be complementary in different regions of the $|U_{eH}|^2$ and m_{ν_H} phase spaces. By combining both approaches, we anticipate observing at least a handful of signal events across most of the parameter space of $10^{-6} < |U_{eH}|^2 < 1$ and 2 MeV $< m_{\nu_H} <$ 15 MeV, assuming a 500-ton solar neutrino experiment operating for one year. Key variables, such as the energy spectra of ν_e or e^+e^- and ν_e solar angle, are also discussed to help distinguish the signal from major backgrounds, such as solar neutrino events.

Keywords: heavy sterile neutrino, solar neutrino experiments, beyond standard model

DOI: 10.1088/1674-1137/ae9929 **CSTR:** 32044.14.ChinesePhysicsC.50113003

I. INTRODUCTION

The observation of neutrino flavor oscillations implies non-zero neutrino masses, marking one of the most significant discoveries in particle physics in the last few decades, as it lies beyond the predictions of the Standard Model (SM) of particle physics. Precisely determining the neutrino masses and exploring new physics models to explain their non-zero values will remain a central focus of particle physics research in the coming decades.

Theoretically, only left-handed neutrinos were introduced in the SM at its time of establishment, as right-handed neutrinos were considered to be unnecessary and would be invisible (or "sterile," meaning no weak or electromagnetic interactions). Owing to the absence of right-handed neutrinos, neutrinos are unable to acquire mass from Yukawa couplings as other fermions do; therefore, the SM predicts that all neutrinos are massless. Experimentally, it is found that neutrino masses are not only non-zero but also exceptionally small: direct measurements from β decay experiments [1] and indirect constraints from Cosmological surveys [2, 3] both give an upper limit on the neutrino mass below 0.5 eV, which is more than six orders of magnitude smaller than the masses of other fermions in the SM.

To explain the non-zero mass of neutrinos, new ingredients must be added to the SM, which can be either new particles, new symmetries, or other extensions. Among the many neutrino mass models, one convenient method is to add right-handed neutrinos to the SM. With right-handed neutrinos, neutrino masses can arise in various ways, such as Dirac masses, similar to other fermions in the SM, or Majorana masses in the type-I seesaw mechanism [4−6], where the former would require extremely small Yukawa couplings (less than 10^{-12}) to explain the observed small neutrino masses, whereas the latter allows for larger couplings by introducing heavy sterile neutrinos that effectively suppress active neutrino masses.

Although sterile neutrinos with extremely large

Received 22 January 2026; Accepted 12 August 2026; Accepted manuscript online 13 August 2026

* Supported by the National Key Research and Development Plan of China (2022YFA1604700), the National Natural Science Foundation of China (12521007, 12575108), and the Tsinghua University Initiative Scientific Research Program

† E-mail: zhicaizhang@tsinghua.edu.cn

Content from this work may be used under the terms of the Creative Commons Attribution 3.0 licence. Any further distribution of this work must maintain attribution to the author(s) and the title of the work, journal citation and DOI. Article funded by SCOAP[3] and published under licence by Chinese Physical Society and the Institute of High Energy Physics of the Chinese Academy of Sciences and the Institute of Modern Physics of the Chinese Academy of Sciences and IOP Publishing Ltd

masses (much larger than the weak scale) are preferable to bring neutrino Yukawa couplings to a similar level as that for other fermions in the SM, heavy sterile neutrinos with masses in the range from eV to TeV are also appealing in many aspects. In addition to being accessible to a wide range of experiments, they can address other problems in particle physics, such as the nature of dark matter [7] and mechanism of leptogenesis [8].

In the type-I seesaw model, the mixing between an active neutrino ν_α and sterile neutrino ν_H, $|U_{\alpha H}|^2$, is approximately the ratio between the active and sterile neutrino masses, m_{ν_α}/m_{ν_H}. Because the mass of active neutrinos is observed to be very small (less than ~ 0.5 eV), the mixing parameter would be extremely small for heavy sterile neutrinos, which indicates very tiny production rates of sterile neutrinos with the usual neutrino sources (such as solar, reactor, and accelerator), particularly in the MeV and higher range. However, some variants of the seesaw model may allow large mixing parameters (for example, reference [9]). As a result, searches for heavy sterile neutrinos in the eV to TeV mass range have been performed with a wide range of experiments, from collider experiments to beta decay measurements. Current results have excluded a wide range of $|U_{\alpha H}|^2$ and m_{ν_H} parameter spaces [10], but there is still an ample uncovered phase space up to the seesaw limit ($|U_{\alpha H}|^2 \sim m_{\nu_\alpha}/m_{\nu_H}$). This paper aims to discuss methods to further extend the sensitivity in the MeV mass range with solar neutrino detectors (currently in operation or under construction).

II. PRODUCTION AND DECAY OF HEAVY STERILE NEUTRINO

Heavy sterile neutrinos (ν_H) with masses of a few MeV can be produced from solar neutrinos (ν_e) through active-sterile neutrino mixing, for example, from ^{8}B solar neutrino as a primary source

$$^8\mathrm{B} \rightarrow {}^8\mathrm{Be}^* + e^+ + \nu_e \rightarrow {}^8\mathrm{Be}^* + e^+ + \nu_H. \tag{1}$$

The flux of ν_H from such a decay chain is proportional to the ^{8}B solar neutrino flux and mixing parameter $|U_{\alpha H}|^2$, scaled by a mass-dependent phase-space factor, as follows:

$$\Phi_{\nu_H}(E) = |U_{eH}|^2 \sqrt{1-\left(\frac{m_{\nu_H}}{E}\right)^2}\,\Phi_{^8\mathrm{B}}(E), \tag{2}$$

where m_{ν_H} and E are the mass and energy of the heavy sterile neutrino, respectively. Using Eq. (2) and the ^{8}B solar neutrino spectrum from [11], we can plot the energy spectra of ν_H from the ^{8}B decay for different ν_H masses, as shown in Fig. 1.

The objective of this work is to explore possible methods to extend the discovery potential of such heavy sterile neutrinos with a mixing parameter $|U_{eH}|^2$ much smaller than 1, getting as close as possible to the seesaw limit (for MeV mass, the seesaw limit is around $|U_{eH}|^2 \sim 10^{-7}$ or even smaller). With such a small mixing parameter, the deficit of ^{8}B solar neutrino owing to mixing with sterile neutrino will be practically invisible to a solar neutrino detector of a few hundred tons (which has a daily ^{8}B solar neutrino event rate of approximately one). As a result, the remainder of this paper will discuss the direct search for heavy sterile neutrinos from ^{8}B decay.

ν_H with a mass heavier than two times the electron mass can decay into an e^+e^- pair plus a left-handed neutrino ν_e. The Feynman diagrams for the production of a heavy sterile neutrino from ^{8}B solar neutrino and its subsequent decay are shown in Fig. 2.

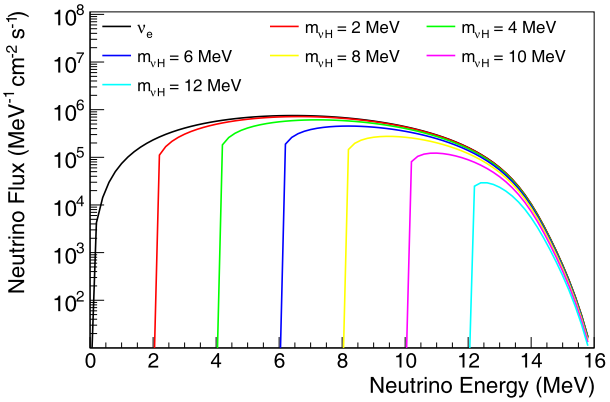


Fig. 1. (color online) Energy spectra of ν_H with different masses emitted from ^{8}B decay in the Sun. The spectra are based on the ^{8}B left-handed solar neutrino spectrum (ν_e in the plot, taken from [11]) and are suppressed by the mixing parameter $|U_{eH}|^2$ and phase-space factor according to Eq. (2), where $|U_{eH}|^2 = 1.0$ in the spectra shown in this plot.

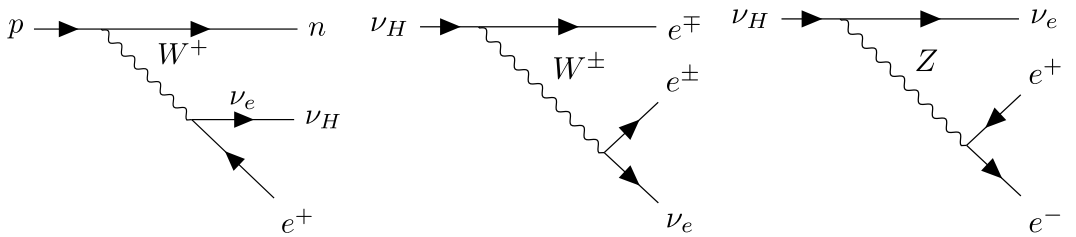


Fig. 2. Feynman diagrams of ν_H production from solar ^{8}B decay and its decay $\nu_H \rightarrow e^+e^-\nu_e$ via $W^\pm$ or Z boson exchange.

In addition to the $\nu_H \to e^+e^-\nu_e$ decay, ν_H can also decay into three neutrinos (ν_e) via Z boson exchange, as well as radiatively decay into $\nu_e+\gamma$ through a W and lepton loop. The width of the $\nu_H \to \nu_e+\gamma$ decay is negligible when compared with that of $e^+e^-\nu_e$ or three-neutrino decay. Calculating the matrix element for ν_H decaying into three active neutrinos is straightforward, and after phase space integration, we obtain the width in the following form:

$$\Gamma_{3\nu_e} = \frac{G_F^2}{192\pi^3} m_{\nu_H}^5 |U_{eH}|^2. \tag{3}$$

The width of $\nu_H \to e^+e^-\nu_e$ is similar to that of $\nu_H \to 3\nu_e$, with minor differences due to the mixed vector and vector-axial terms and non-negligible electron mass. The exact value of $\Gamma_{e^+e^-\nu_e}$ can be found in [12]. For ν_H with a sufficiently large mass ($m_{\nu_H} \gg m_e$), the ratio of $\Gamma_{e^+e^-\nu_e}$ to $\Gamma_{3\nu_e}$ is approximately

$$\frac{\Gamma_{e^+e^-\nu_e}}{\Gamma_{3\nu_e}} \approx \frac{1}{4}(1-4\sin^2\theta_w+8\sin^4\theta_w) \approx 0.6 \tag{4}$$

From the width calculations above, we can determine the proper lifetime of ν_H decay as a function of its mass and the mixing parameter $|U_{eH}|^2$, as shown in Fig. 3. ν_H with a small mass and small mixing parameter can have an extremely long lifetime, which is evident from Eq. (3). For the lower left corner (small mass and small mixing parameter), only a small fraction of ν_H decays before reaching our detector on Earth, whereas for the upper right corner (large mass and large mixing parameter), most of ν_H decays within the orbit of Earth.

Because ν_H itself does not produce detectable signals in most traditional neutrino detectors (except those designed to detect extremely weak signals such as coherent elastic neutrino-nucleus scattering, as reported in [13]), direct searches for ν_H typically rely on detecting its decay products. These could be either the e^+e^- pair or ν_e shown in Fig. 2, as illustrated in Fig. 4.

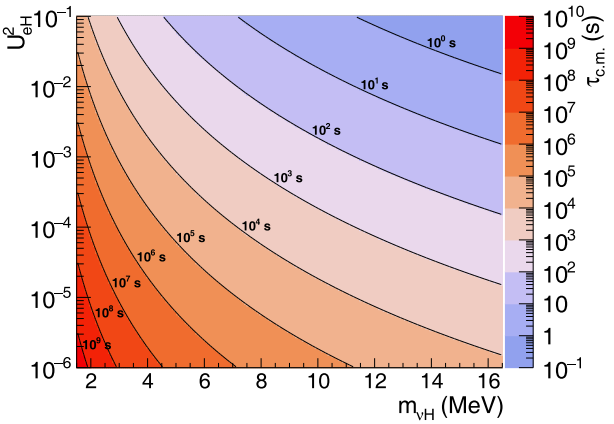


Fig. 3. (color online) Proper lifetime ($\tau_{\text{c.m.}} = 1/\Gamma_{\text{total}}$) of ν_H as a function of mass m_{ν_H} and mixing parameter $|U_{eH}|^2$.

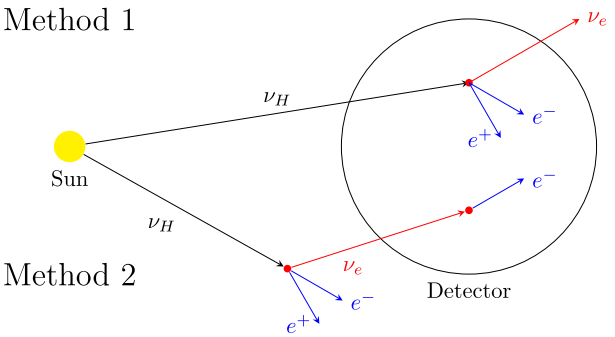


Fig. 4. (color online) Two detection methods for heavy sterile neutrinos: (1) e^+e^- pair detection from ν_H decays occurring inside the detector and (2) ν_e detection from ν_H decays occurring outside the detector.

- **Method 1**: If ν_H decays inside the detector, we can search for the e^+e^- signal event within the detector.

- **Method 2**: If ν_H decays before reaching the detector, the detectable signal would be a ν_e event in our detector.

The remainder of this paper explores both methods and discusses their complementary sensitivity across the full phase space of m_{ν_H} and $|U_{eH}|^2$.

III. METHOD 1: SEARCH FOR ν_H USING THE e^+e^- SIGNAL

To estimate the sensitivity of ν_H searches using the e^+e^- signal from its decay, we calculate and present the event rates for both signal and major background events, along with the distribution of a key discriminating variable—the total energy deposition spectrum—across the entire m_{ν_H}-$|U_{eH}|^2$ parameter space under investigation.

The signal event rate can be estimated by calculating the ν_H decay rate within the detector. For ν_H with a production rate R_0 at the Sun (source), lifetime τ, Sun-to-Earth time of flight t, time of flight inside the detector dt, and detector solid angle dΩ relative to the Sun, the ν_H decay rate inside the detector is given by

$$R = R_0 \frac{\mathrm{d}\Omega}{4\pi} \frac{\mathrm{d}t}{\tau} \exp\left(\frac{-t}{\tau}\right). \tag{5}$$

To analyze the rate variation across different regions of the m_{ν_H}-$|U_{eH}|^2$ parameter space, we can treat τ as the primary variable of change, as t and dt remain relatively constant for different m_{ν_H} and $|U_{eH}|^2$ values. By taking the derivative dR/dτ of Eq. (5), we find that R increases with τ until $\tau = t$ (approximately 500 s in most cases), after which R decreases as τ continues to increase.

Combining this observation with the lifetime distribution shown in Fig. 3 and source rate (R_0) from Eq. (2), we can conclude the following:

1. The ratio R/R_0 (total signal efficiency) peaks near the $\tau = 500$ s contour in Fig. 3 and reaches the minima at both corners (lower left and upper right).

2. According to Eq. (2), R_0 is maximized in the upper left corner of Fig. 3 and minimized in the lower right corner.

3. Consequently, the contour lines of the signal event rate R in the $|U_{eH}|^2$ vs. m_{ν_H} plane resemble a crest aligned with the $\tau = 500$ s contour (approximately diagonal in Fig. 3), with the maximum at the upper left corner and minimum at the lower right corner.

The exact values of R in Eq. (5) can be obtained by substituting R_0 with the total flux from Eq. (2) and calculating the time of flight (t or dt) using

$$t = \frac{m_{\nu_H}}{E_{\nu_H}} \frac{D}{\beta c}, \tag{6}$$

where D represents the travel distance (Sun-Earth distance for t or detector size for dt). For a 500-ton spherical detector on Earth, we calculated the expected e^+e^- signal event rates from ν_H decay across various m_{ν_H} and $|U_{eH}|^2$ values, as summarized in Table 1. These results are visualized in the top panel of Fig. 5, showing the expected crest-like contour pattern in the signal rate distribution.

The primary background for e^+e^- signals from ν_H decays in solar neutrino detectors comes from the electrons produced through the elastic scattering of solar neutrinos with detector materials. The key distinction between ν_H signals and solar neutrino backgrounds lies in their final states: ν_H decays produce e^+e^- pairs, whereas background events generate single electrons.

For Cherenkov detectors, e^+e^- pairs can potentially be distinguished from single electrons when their opening angle is sufficiently large. Scintillation detectors, however, must rely on differences in the total deposited energy spectra for signal-background separation. Advanced slow scintillation detectors with directional sensitivity [14] can leverage both energy spectra and opening angle information to optimize the signal-to-background ratios.

Table 1. Expected event rate (per year) of e^+e^- pairs from $\nu_H \to \nu_e e^+e^-$ decays occurring within the detector, shown for different mixing parameters $|U_{eH}|^2$ and ν_H masses, assuming a 500-ton neutrino detector.

$\lvert U_{eH}\rvert^2$	M_{ν_H}/MeV					
	2	4	6	8	10	12
10^{-1}	9.7×10^5	3.8×10^7	2.4×10^5	0	0	0
10^{-2}	1.0×10^4	1.2×10^6	2.4×10^6	3.6×10^4	0	0
10^{-3}	1.0×10^2	1.5×10^4	1.1×10^5	1.2×10^5	9.2×10^3	2.2
10^{-4}	1.0	1.5×10^2	1.4×10^3	3.7×10^3	3.2×10^3	4.5×10^2
10^{-5}	0	1.5	14.1	43.5	58.0	25.8
10^{-6}	0	0	0.1	0.4	0.6	0.3

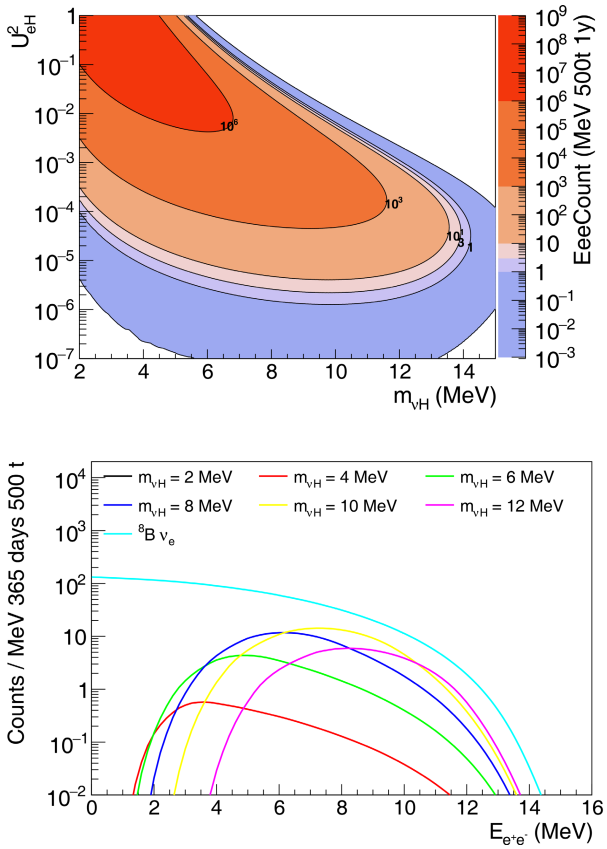


Fig. 5. (color online) Top: Count rate (per year) of e^+e^- signal from ν_H decay inside a 500-ton detector on Earth as a function of m_{ν_H} and $|U_{eH}|^2$. Bottom: Energy spectrum of e^+e^- signal from ν_H decay, along with the energy spectrum of the major background (scattered electron in the detector from solar ^{8}B neutrino). Different values of ν_H mass are shown, with $|U_{eH}|^2 = 10^{-5}$.

We now calculate the expected energy spectrum of e^+e^- pairs from ν_H decays and compare it with solar neutrino background spectra. The differential width for $\nu_H \to e^+e^-\nu_e$ decay can be found in [15], which takes the form

$$\frac{\mathrm{d}\Gamma}{\mathrm{d}E\,\mathrm{d}\cos\theta} = \Gamma_{\rm total}(f_1 + \zeta|\vec{P}|f_S\cos\theta), \tag{7}$$

where E and θ represent the energy and emission angle of ν_e in the ν_H rest frame; $\Gamma_{\rm total}$ is the total decay width; f_1 and f_S are functions of m_{ν_H} and E; $|\vec{P}| \approx \beta$ denotes the ν_H

polarization; and $\zeta = +1$ (-1) for ν_H $(\bar{\nu}_H)$.

Using the ν_e energy spectrum from Eq. (7) in the ν_H rest frame, we compute the total e^+e^- energy spectrum in the laboratory frame. The e^+e^- spectral shape varies with m_{ν_H}, as shown in the bottom panel of Fig. 5. This plot compares the e^+e^- spectra from ν_H decays (normalized to the rates in a 500-ton neutrino detector) with the electron spectra from ^{8}B solar neutrino elastic scattering. Distinct spectral peaks emerge at the tail of the background spectrum for most ν_H masses, suggesting that precise energy measurements in scintillation detectors should enable excellent signal-background discrimination through spectral fitting.

By combining the information from the top and bottom plots of Fig. 5, we expect to observe at least a handful of $\nu_H \to e^+e^-\nu_e$ events by the detection of e^+e^- inside the detector for most regions where $|U_{eH}|^2 > 10^{-6}$ and $2\,\text{MeV} < m_{\nu_H} < 15\,\text{MeV}$. Using the e^+e^- total energy spectrum, the Borexino experiment excluded some of the phase space in the above region of $|U_{eH}|^2$ and m_{ν_H} using 446 days of Borexino data [16]. Future solar neutrino observatories with larger central volumes and direction measurement capabilities—and therefore better separation of e^+e^- from single electron events—such as the Jinping Neutrino Experiment (JNE) [14, 17], could further extend the sensitivity to ν_H in these regions.

The uncovered regions in the phase space are the lower-left and upper-right corners of $|U_{eH}|^2$ and m_{ν_H}, as shown in Fig. 5, where ν_H is either too short-lived or too long-lived, leading to insufficient ν_H decays inside the detector. To cover those regions, one must search for ν_H that decays outside the detector, for which the only method is to detect the ν_e from ν_H decay, which will be discussed in the next section.

Furthermore, to obtain the energy and angular distributions of the decay products, we employ MadGraph aMC@NLO [18] to generate the decay events in the rest frame of the heavy neutrino ($\nu_H \to \nu_e e^+e^-$). These events are subsequently boosted to the laboratory frame by sampling from the predicted ν_H energy spectrum (Fig. 1). As shown in Fig. 6, for the majority of events, the opening angle of the e^+e^- pair is sufficiently large to allow these pairs to be distinguished from background events containing single electrons. Moreover, as the mass of the right-handed neutrino increases, the proportion of events with a larger opening angle also increases.

IV. METHOD 2: SEARCH FOR ν_H USING THE ν_e SIGNAL

For regions of $|U_{eH}|^2$ and m_{ν_H} where ν_H is too short-lived, the majority of ν_H will decay before they reach the orbit of Earth. Among the decay products, the only particle that can reach our detector on Earth is the active neutrino ν_e. The ν_e from ν_H decay is similar to solar neutrinos, making it challenging to distinguish this signal from the solar neutrino background. No such search has been performed with existing solar neutrino detectors worldwide.

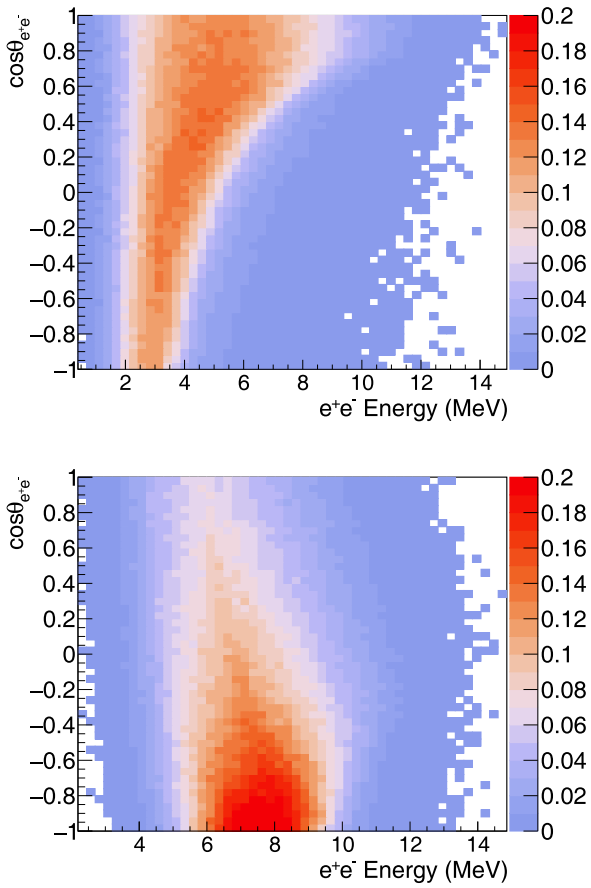


Fig. 6. (color online) Distribution of opening angle and energy of e^+e^- pairs from ν_H decay with $|U_{eH}|^2 = 10^{-5}$. Top: $m_{\nu_H} = 4$ MeV; Bottom: $m_{\nu_H} = 10$ MeV

This paper explores two variables to differentiate ν_e from the ν_H decay and solar neutrino background: the ν_e energy and direction. The signal ν_e is from ν_H decay, and ν_H itself is from a solar neutrino by active-sterile mixing; therefore, the energy of the signal ν_e should be significantly lower than the original solar neutrino energy. Regarding the ν_e direction, the solar neutrino we detect on Earth always comes from the Sun, but ν_H can decay anywhere in space and generate ν_e that travels to Earth. Consequently, the angle between the ν_e direction and Sun-Earth line (θ_{Sun}) should be different for the signal and background.

The calculation of the energy and angular distribution of ν_e from the ν_H that reaches the detector on Earth begins with the energy and angular distribution of all emitted ν_e from ν_H, as shown in Eq. (7). From Eq. (7), we simply need to integrate over all ν_H decay points in space and all ν_e emission angles to collect all ν_e that can reach our detector on Earth. Fig. 7 shows two typical situations

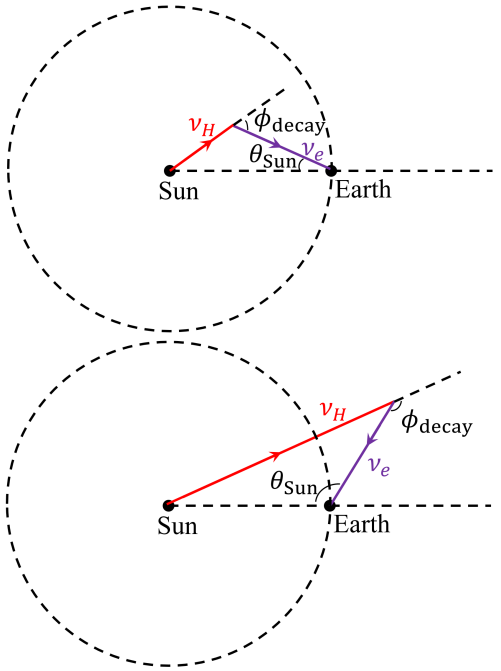


Fig. 7. (color online) Definitions of angles $\phi_{\rm decay}$ (emission angle) and $\theta_{\rm Sun}$ (solar angle) for ν_H decay in flight and subsequent arrival of the decay product ν_e at the detector on Earth. Different methods of ν_H decays are shown: ν_H decay inside the orbit of Earth (top plot) and ν_H decay outside the orbit of Earth (bottom plot).

of the decay of ν_H with ν_e entering the detector on Earth, where ν_H can either decay inside or outside the orbit of Earth. Two angles are defined and illustrated in Fig. 7:

1. ν_e emission angle $\phi_{\rm decay}$: angle between the directions of ν_H and ν_e. This angle is the same as the angle θ in Eq. (7) (except that θ in Eq. (7) is in the ν_H rest frame, and $\phi_{\rm decay}$ is in the lab frame).

2. ν_e solar angle $\theta_{\rm Sun}$: angle between ν_e direction and the Sun-Earth line.

The 3-dimensional integration over all space can be simplified to a 1-dimensional integration when calculating the energy and $\theta_{\rm Sun}$ distributions of all ν_e that reach our detector on Earth. The simplification is based on the fact that all detectors placed on any point on the spherical surface S with the Sun as the center and the Sun-Earth distance as the radius should have the same energy and $\theta_{\rm Sun}$ distributions as those of ν_e. Therefore, we need to consider only the decay vertices along a straight line from the Sun to infinity, integrating over decays where ν_e intersects with the surface S. The energy distribution of these intersecting ν_e corresponds directly to the energy spectrum of our signal for a neutrino detector. Additionally, the angle between the direction of ν_e and the line from the Sun to their intersection gives the desired $\theta_{\rm Sun}$ distribution.

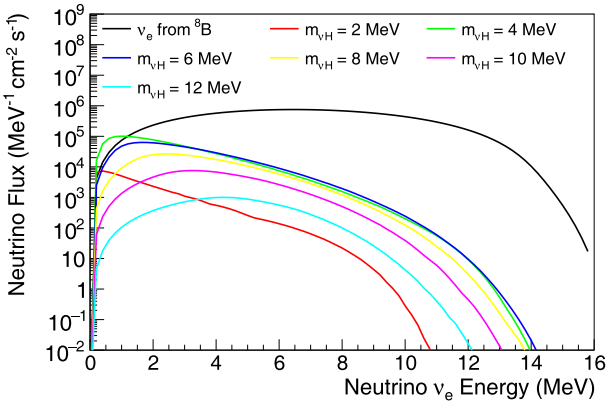


Fig. 8. (color online) Energy spectra of ν_e from ν_H decay that reach the detector on Earth for different values of m_{ν_H} with $|U_{eH}|^2 = 0.1$. The plot also shows the energy spectrum of the background ^{8}B solar neutrino (black curve).

Figure 8 shows the energy spectra of ν_e from ν_H decay that reach the detector on Earth. As expected, the signal ν_e from this decay is much softer than the background ^{8}B solar neutrino, peaking below 5 MeV. Distinguishing these low-energy ν_e from background solar neutrinos is challenging, as the electron energy from the elastic scattering of ^{8}B also peaks at low energies, as shown in Fig. 5. A good signal-to-background ratio will significantly enhance ν_e detection through charged-current interactions (as proposed in [19, 20]), where the recoil energy closely correlates with the neutrino energy.

The solar angle $\theta_{\rm Sun}$ distinguishes the signal ν_e (from ν_H decay) from the solar neutrino background. The background solar neutrinos have a solar angle of zero, as they originate from the Sun. Figure 9 illustrates the distribution of the solar angle for the signal ν_e based on specific values of m_{ν_H} and $|U_{eH}|^2$. For a signal ν_e, there is a small but significant tail with large solar angles that can exceed the typical angular resolution limits (around 25°) of standard detectors. The bottom plot in Fig. 9 shows that for $|U_{eH}|^2 > 10^{-2}$, there is a large region with at least 10% of ν_e events having a solar angle $\theta_{\rm Sun} > 25°$ (or $\cos\theta_{\rm Sun} < 0.9$), allowing them to be distinguished from the background neutrinos by major detectors capable of direction measurement.

Considering the ν_e-electron scattering cross section (approximately 9.4×10^{-45} cm^2 for $E_{\nu_e} = 10$ MeV), we can estimate the expected event count rate for detecting ν_e signals from ν_H decay, as shown in Fig. 10. In most of the phase space where $|U_{eH}|^2 > 10^{-2}$, we expect to observe at least a few ν_H events by detecting ν_e from its decay, using about one year of data from a 500-ton solar neutrino detector. Unlike Fig. 5, much of this phase space cannot be explored by searching for e^+e^- signals owing to the short lifetime of ν_H.

In addition, the solar angle cosine distribution of e^-

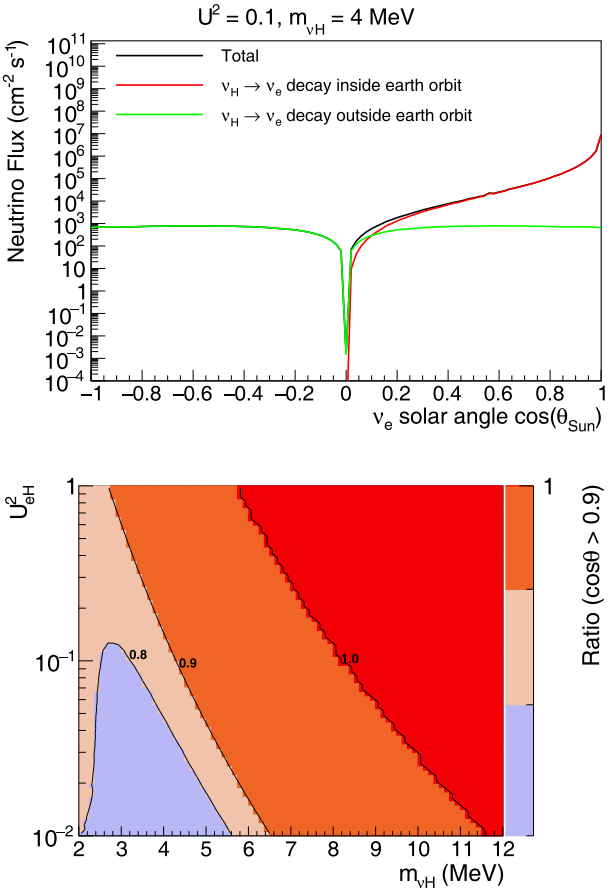


Fig. 9. (color online) Top: Distribution of $\cos\theta_{\rm Sun}$ of ν_e from ν_H decay and subsequent arrival at the detector on Earth with $m_{\nu_H} = 4$ MeV and $|U_{eH}|^2 = 0.1$. The distributions for ν_H decay inside and outside the orbit of Earth are shown separately. Bottom: Ratio of ν_e with $\cos\theta_{\rm Sun} > 0.9$ for different m_{ν_H} and $|U_{eH}|^2$.

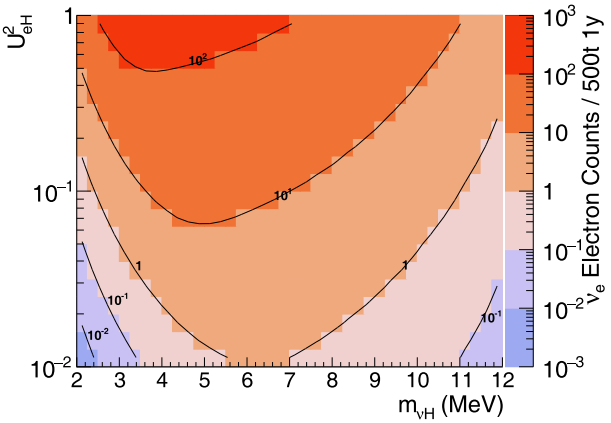


Fig. 10. (color online) Event rate of ν_e-electron elastic scattering per year with a 500-ton detector for ν_e signal from ν_H decay.

from ν_e-e^- scattering is obtained and presented in Fig. 11. Based on Fig. 11, it is expected that scattered electrons with large solar angles are those with low energies (below 2 MeV for $\cos(\theta_{\rm Sun}) < 0.9$). At such low kinetic energies, it remains challenging to utilize the directional information to effectively distinguish these signals from the ^{8}B solar neutrino background.

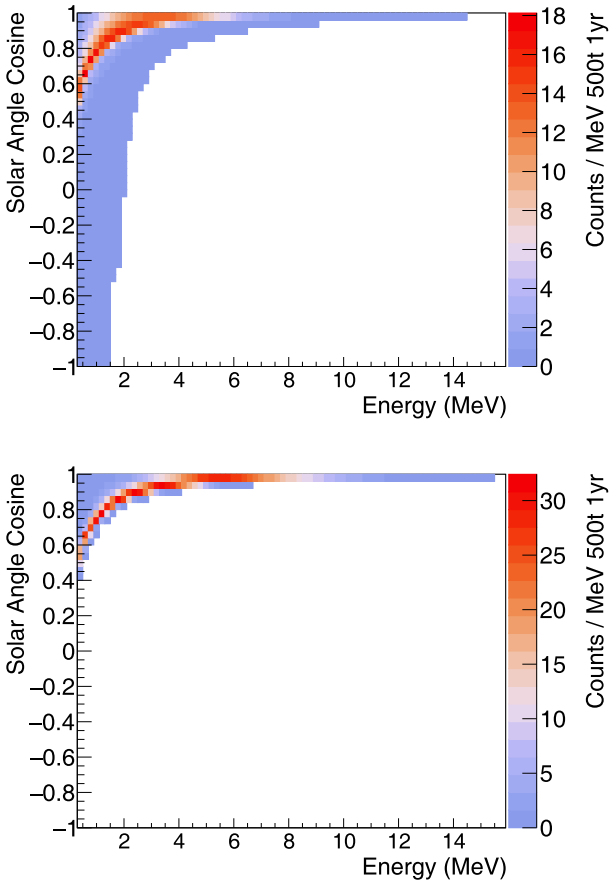


Fig. 11. (color online) Count rate distribution of solar angle cosine and scattering electron energy with $m_{\nu_H} = 4$ MeV and $|U_{eH}|^2 = 0.1$. Top: signal ν_e from ν_H decay; Bottom: ^{8}B solar neutrino background. The background is confined to $\cos\theta_{\rm Sun} \gtrsim 0.4$ by the elastic-scattering kinematics, whereas the signal populates the full $\cos\theta_{\rm Sun}$ range, including the backward ($\cos\theta_{\rm Sun} < 0$) region.

V. SENSITIVITIES

To quantify the discovery potential across the parameter space, we evaluate the expected sensitivity using the profile likelihood method with Asimov data sets [21].

For method 1, the signal S_i is the e^+e^- energy spectrum from $\nu_H \to \nu_e e^+ e^-$ decays inside the detector volume, whereas the background B_i is the ^{8}B solar neutrino–electron elastic scattering spectrum. Both the signal and background are convolved with a Gaussian energy resolution of $5\%/\sqrt{E[\rm MeV]}$ to account for the detector response.

We construct an Asimov data set $n_i = B_i$ and define the binned Poisson likelihood, as follows:

$$\mathcal{L}(\mu,\beta)=\prod_i \text{Poisson}\left(n_i|\mu S_i+\beta B_i\right), \tag{8}$$

where μ is the signal strength and β is an unconstrained nuisance parameter that absorbs the systematic uncertainty in the solar neutrino flux. The energy spectra are binned with a width of 0.2 MeV, and the fit is restricted to the window $4.8 < E_{ee} < 12.8$ MeV (40 bins) to suppress the environmental and cosmogenic backgrounds (e.g., ^{208}Tl and ^{11}C) that dominate at lower energies.

For each point $(m_{\nu_H},|U_{eH}|^2)$, we test the nominal signal hypothesis ($\mu=1$) against the background-only hypothesis ($\mu=0$) via the profile likelihood ratio [21]

$$q_1=-2\ln\frac{\mathcal{L}(1,\hat{\beta}_1)}{\mathcal{L}(0,\hat{\beta}_0)}, \tag{9}$$

where $\hat{\beta}_\mu$ is the maximum likelihood estimate of β for a fixed μ. Under Wilks' theorem, q_1 follows a χ^2 distribution with one degree of freedom. A parameter point is excluded at 90% C.L. if $q_1 > 2.71$. The resulting expected exclusion contour is shown as the solid blue line in Fig. 12.

To further improve the sensitivity, we also examine the last analysis in section III, which exploits the opening angle $\theta_{e^+e^-}$ between the electron and positron from ν_H decay. Neutrino detectors with directional sensitivity such as JNE can achieve an angular resolution of approximately 25°[1)], corresponding to $\cos\theta_{e^+e^-}\lesssim 0.9$. Therefore, the e^+e^- opening angle distribution is smeared with a Gaussian angular resolution of 25° to account for the detector's directional response. A selection of $\cos\theta_{e^+e^-}<0.9$ is also applied, and the corresponding improved exclusion sensitivity is shown as the solid cyan line in Fig. 12.

For method 2, which searches for ν_e from ν_H decay via ν_e–electron elastic scattering, the same statistical approach is applied using a two-dimensional template fit in the reconstructed electron energy E_e and solar angle $\cos\theta_{\text{Sun}}$. The signal includes ν_e from ν_H decays that undergo elastic scattering in the detector. The background is the standard ^{8}B solar neutrino elastic scattering, with the component that oscillated into ν_H subtracted for consistency. The energy spectrum and angular distribution are both smeared in a similar way as for method 1. The two-dimensional template is binned in the reconstructed electron solar angle $\cos\theta_{\text{Sun}}$ (50 uniform bins over $[-1,1]$) and energy E_e (0.2 MeV bins spanning the full range). The expected 90% C.L. exclusion contour from method 2 is shown as the solid orange line in Fig. 12.

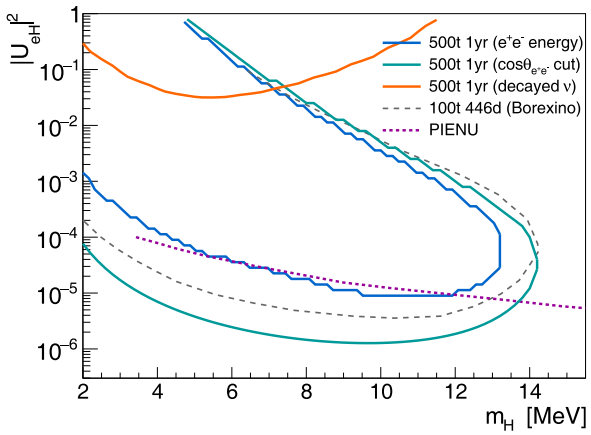


Fig. 12. (color online) Expected 90% C.L. exclusion contours for a 500-ton detector with one year of exposure. The solid blue curve shows the sensitivity from method 1 using the e^+e^- energy spectrum alone. The solid cyan curve shows the improved sensitivity from method 1 using the opening angle $\theta_{e^+e^-}$ with the $\cos\theta_{e^+e^-}<0.9$ selection. The solid orange curve shows the sensitivity from method 2, searching for ν_e from ν_H decay via elastic scattering. The gray dashed curve is the published Borexino exclusion [16]. The magenta dotted curve shows the PIENU constraint [22].

For comparison, the Borexino constraint, which has already excluded a portion of the parameter space using 446 days of data [16], is also shown as the gray dashed curve in Fig. 12. Complementary constraints in this mass range have also been reported from laboratory $\pi\to e\nu$ decay searches (PIENU) [22, 23], which probe the ν_H produced in pion decay rather than in the Sun.

VI. SUMMARY

Solar neutrino experiments, particularly those with new designs that provide good energy and direction measurements, are promising for heavy sterile neutrino searches in the MeV mass range. In this range, ν_H can decay into an e^+e^- pair plus an active neutrino ν_e. This paper presents two methods based on this decay: one focuses on detecting ample e^+e^- signals from ν_H decays with an intermediate lifetime, while the other aims to find ν_e from short-lived ν_H decays. The estimated signal and background event yields indicate the complementary sensitivity of both methods. Key variables to distinguish the ν_H signal from solar neutrino events are proposed along with their distributions. By combining these methods, it is expected to be sensitive in most of the phase space with $|U_{eH}|^2>10^{-6}$ and $2\text{ MeV}<m_{\nu_H}<15$ MeV using the data from a 500-ton detector over one year.

1) For JNE, a slow liquid-scintillator detector, the direction is reconstructed from the Cherenkov component of the light; in the simulations of Ref. [14], an angular resolution of better than 25° is reached at electron energies above 6 MeV, the exact value depending on the scintillator. The resolution improves at higher energies. A fixed 25° resolution is adopted for sensitivity estimates in this work.

References

[1] M. Aker *et al*. (KATRIN Collaboration), Science **388**, 180 (2025), arXiv: 2406.13516
[2] A. G. Adame *et al*. (DESI Collaboration), JCAP **02**, 021 (2025), arXiv: 2404.03002
[3] N. Aghanim *et al*. (Planck Collaboration), A&A **641**, A6 (2020), arXiv: 1807.06209
[4] M. Gell-Mann, P. Ramond, and R. Slansky, Conf. Proc. C **790927**, 315 (1979), arXiv: 1306.4669[hep-th]
[5] T. Yanagida, Conf. Proc. C **7902131**, 95 (1979)
[6] R. N. Mohapatra and G. Senjanović, Phys. Rev. Lett. **44**, 912 (1980)
[7] T. Asaka, S. Blanchet, and M. Shaposhnikov, Phys. Lett. B **631**, 151 (2005), arXiv: hep-ph/0503065
[8] E. K. Akhmedov, V. A. Rubakov, and A. Y. Smirnov, Phys. Rev. Lett. **81**, 1359 (1998), arXiv: hep-ph/9803255
[9] X. G. He, S. Oh, J. Tandean *et al*., Phys. Rev. D **80**, 073012 (2009), arXiv: 0907.1607
[10] P. D. Bolton, F. F. Deppisch, and P. Dev, JHEP **2020**, 170 (2020), arXiv: 1912.03058
[11] J. N. Bahcall, E. Lisi, D. E. Alburger *et al*., Phys. Rev. C **54**, 411 (1996)
[12] D. Gorbunov and M. Shaposhnikov, JHEP **10**, 015 (2007)
[13] XENON Collaboration, Phys. Rev. Lett. **133**, 191002 (2024)
[14] W. Luo, Q. Liu, Y. Zheng *et al*., JINST **18**(02), P02004 (2023), arXiv: 2209.13772
[15] R. E. Shrock, Phys. Rev. D **24**, 1275 (1981)
[16] Borexino Collaboration, Phys. Rev. D **88**, 072010 (2013), arXiv: 1311.5347[hep-ex]
[17] J. F. Beacom, S. Chen, J. Cheng *et al*., Chin. Phys. C **41**, 023002 (2017), arXiv: 1602.01733
[18] J. Alwall, R. Frederix, S. Frixione *et al*., JHEP **2014**, 079 (2014), arXiv: 1405.0301
[19] Y. Liang, H. Sun, and Z. Wang, (2025), arXiv: 2505.13926
[20] W. Shao, W. Xu, Y. Liang *et al*., Eur. Phys. J. C **83**, 799 (2023), arXiv: 2203.01860
[21] G. Cowan, K. Cranmer, E. Gross, *et al*., Eur. Phys. J. C **71**, 1554 (2011)
[22] A. Aguilar-Arevalo, M. Aoki, M. Blecher *et al*., Phys. Rev. D **97**, 072012 (2018)
[23] D. A. Bryman and R. Shrock, Phys. Rev. D **100**, 053006 (2019)